Applied Surface Science 617 (2023) 156563

Contents lists available at ScienceDirect

Applied Surface Science

journal homepage: www.elsevier.com/locate/apsusc

Full Length Article

Design and characterization of polyurethane based electrospun systems modified with transition metals oxides for protective clothing applications

Gianluca Viscusi [a], Elena Lamberti [a], Francesca D'Amico [a], Loredana Tammaro [b], Giovanni Vigliotta [c], Giuliana Gorrasi [a,*]

[a] Department of Industrial Engineering, University of Salerno, via Giovanni Paolo II, 132, 84084 Fisciano (SA), Italy
[b] Laboratory of Nanomaterials and Devices (SSPT-PROMAS-NANO), ENEA-C.R. Portici, Piazzale Enrico Fermi 1, 80055 Portici (NA), Italy
[c] Department of Chemistry and Biology, University of Salerno, Via Giovanni Paolo II, 132, 84084 Fisciano (SA), Italy

ARTICLE INFO

Keywords:
Polyurethane
Electrospinning
Protective clothing
UV photodegradation
Surface coating

ABSTRACT

This paper reports the design and the fabrication of novel fiber membranes based on electrospun polyurethane (PU) fibers modified with copper and zinc oxide as potential systems for protective clothing. A one-step in-situ methodology is proposed to modify the PU systems. The modified PU membranes are widely characterized in terms of spectroscopic, morphological, thermal and barrier properties. Evaluation of surface charge and analysis of retention degree, obtained by testing four model systems (H_2O, H_2O/NaOH, lemon juice and sweat simulant), are even carried out. Then, to evaluate the protection against UV rays, weathering tests are accomplished while the carbonyl index gives a proof of the improved UV stability. The estimation of ultraviolet protection factor allowed to prove the total resistance to UV-A and UV-B rays. Finally, cytostatic effect against $Gram^+$ and $Gram^-$ bacteria is evaluated. The reported results allow for stating that the designed materials show great potential as high-performance systems for protective clothing applications.

1. Introduction

Nowadays, there is a wide interest in the design of multifunctional textiles. For example, since ultraviolet radiation is considered harmful, the development of ultraviolet (UV)-blocking fabrics for outdoors uses has received increasing attention. In fact, UV rays can cause the formation of free radicals and the long-term exposure of human skin can induce health issues (i.e. aging, DNA damage, skin reddening, acne, skin cancer) [1]. Apart from the health concern, UV radiation can even be responsible for discoloration of dyes pigments, weathering, yellowing of plastics and loss of gloss and mechanical properties of textiles [2]. As a consequence, the fabrication and design of UV-protective materials has become an important issue in different applications such as industry, health-care, military [3,4] since, for example, agricultural or construction workers can undergo continuously to a high exposure to UV radiation over extended periods of time [5,6]. In order to overcome that, appropriate textiles are designed as a protection measure for UV rays and skin cancer prevention. In the textile industries, there are already available inorganic and organic UV absorbers [7] used to develop UV protective materials such as sunscreen, coatings and films [8]. Among inorganic ones, some chemical compounds typically based on metal oxide can efficiently absorb UV radiation showing good heat-resistance properties. Some examples are TiO_2, CeO_2 and ZnO [7,9,10]. Moreover, great interest in the antibacterial finishing of fabrics for practical applications has been observed in the last decades [11]. For example, textile materials used in some environments are conducive to cross-infection or transmission of diseases caused by micro-organisms. In general, antimicrobial properties can be imparted to textile materials by chemical or physical modification of fabrics. Among the different techniques of production of functional textiles, electrospinning is emerging as a good candidate for producing fibrous systems with micro and nanometric dimensions for targeted applications [12–16]. The technique has been widely applied in different technological fields such as wound healing, gas shielding, filtration, protective clothing and tissue engineering applications. [12,17–22]. In the field of textiles and clothing, the potential of electrospun systems is emerging in the last decades since functional clothing materials with novel properties may be produced through the applications of novel technologies [6,23,24]. Many polymers have already been processed by electrospinning to produce fine fibers [6]. Thermoplastic polyurethanes (PUs) are a kind of

* Corresponding author.
E-mail address: ggorrasi@unisa.it (G. Gorrasi).

https://doi.org/10.1016/j.apsusc.2023.156563
Received 18 October 2022; Received in revised form 14 January 2023; Accepted 24 January 2023
Available online 28 January 2023

thermoplastics with the mechanical characteristics of rubber [25–27]. PU elastomers can be regarded as a block copolymers of the $(A\text{-}B)_n$ type with good physical properties, chemical resistance, excellent shock absorption, abrasion resistance, biocompatibility and good processability as well [28–31]. PUs are widely used for many applications such as automotive, coating, shoe soles, adhesives for textile, aerospace, drug delivery and vibration-proofing assemblies [32,33]. Despite their good physical properties, other characteristics such as mechanical performances, resistance to UV light and flammability yet to be further improved to face more hard conditions [34]. Concerning the extreme sensitivity to UV light, it is known that PUs undergo significant structural changes on exposure to UV radiation determining decreasing in their physical and mechanical properties [35,36]. The phenomenon of yellowing is due to the formation of oxidation reaction in the backbone of the materials which induces a modification of physical and chemical characteristics of their surface resulting in color change and degradation [36]. With the aim of improving the properties of PUs based systems for textile applications, hydrothermal synthesis has been proposed to chemically functionalized PU electrospun fibers. Hydrothermal synthesis is a simple, low-cost, energy-saving and environmentally friendly method with the potentiality for large-scale commercialization. The preparation method does not require surfactants or templates and greatly reduces costs and saves resources. The procedure is based on the precipitation of transition metals salts which generates transition metals oxides onto the surface of a polymeric support. Metal oxide particles are shown to degrade chemical and biological warfare compounds as well as to enhance various properties such as mechanical properties, resistance to chemicals, flame retardancy, antibacterial and self-cleaning properties [37]. For example, ZnO is widely used in antibacterial studies [38] and as a UV-blocking agent for fabrics, films of polymers, and personal care products since its non-toxicity, compatibility with skin, and chemical stability under exposure to both high temperatures and UV rays [39]. Copper oxide, besides, is commonly used as antimicrobial agent, due to ability to bind the donor ligands present in the pathogen cells inducing oxidative stress [40]. So, taking into account the properties of the metal oxides, physical properties of modified PU membranes, antimicrobial activity, liquid retention and UV-stability were studied to corroborate and prove the effectiveness of the fabricated systems as novel functional textiles for protective clothing application.

2. Materials & methods

Thermoplastic polyurethane was purchased from Nippon Gohsei. Dimethylformamide (CAS: 68–12-2) tetrahydrofuran (CAS: 109–99-9), copper chloride (CAS: 7447–39-4), zinc nitrate hexahydrate (CAS: 10196–18-6), sodium hydroxide (CAS: 1310–73-2), ammonium hydroxide solution (CAS: 1336–21-6), ammonium chloride (CAS: 12125–02-9), hydrochloric acid solution 37 % v/v (CAS: 7647–01-0), urea (CAS: 57–13-6), lactic acid (CAS: 50–21-5) were purchased from Sigma Aldrich. Lemon juice was purchased from a local supermarket. Sodium chloride (CAS: 7647–14-5) was purchased from Carlo Erba Reagents.

2.1. Electrospinning of PU membrane

Polyurethane polymeric solution was prepared by dissolving PU pellets (20 % w/w) in dimethylformamide/tetrahydrofuran solution (1:1 v/v). The obtained solution was stirred for 10 h at 50 °C and 250 rpm. After that, the PU solution was fed to a 5 mL syringe pump. Electrospinning process parameters are hereafter reported: flow rate = 1 mL/h, voltage = 24 kV, distance needle-collector = 23.5 cm, temperature = 25 °C and relative humidity = 35 %.

2.2. Modification of PU membrane

Modification of PU fibers was achieved through chemical bath precipitation by preparing an aqueous solution (100 mL) of zinc and copper salts (0.036 mol). NH_4Cl was then added (0.0183 mol). The as prepared solution was stirred at 100 °C since the complete solubilization of salts. Then, PU membrane was put into contact with the salt solution in inert atmosphere. Finally, NH_4OH was added (12 mL). The reaction lasts 24 h. After that, the surface modified PU membranes were deeply washed with water and ethanol before drying in vacuum oven at 60 °C for 8 h. The same methodology was applied to modify PU membrane with a combination of copper and zinc (Cu/Zn 1:1 mol/mol). The prepared samples will be hereafter labelled as PU@Cu, PU@Zn and PU@Cu/Zn.

2.3. Techniques of characterization

2.3.1. Analysis of physical properties

To investigate the morphology of the membranes, SEM analysis was carried out. Before the analysis, samples were covered with a thin film of gold by sputtering. Images were acquired by a Phenom ProX microscope, working in high-vacuum mode. Plot profiles were obtained from SEM images through Plot Profile plug-in of Fiji software. Image processing analysis allows to display a two-dimensional graph by selecting an area of roughly 1000 μm^2. The x-axis represents the distance along the line and the y-axis is the pixel intensity.

Surface roughness parameters were evaluated though mathematical equations. R_a (arithmetic average of the absolute values of the profile height deviations from the mean line, recorded within the evaluation length) and RMS (root mean square average of the profile height deviations from the mean line, recorded within the evaluation length (L)) were evaluated through eqs. 1 and 2:

$$R_a = \frac{1}{L} * \int_0^L |Z(x)|dx \quad (1)$$

$$RMS = \left[\frac{1}{L} * \int_0^L Z(x)^2 dx\right]^{1/2} \quad (2)$$

where Z(x) is the profile height function.

X-ray diffraction patterns were taken, in reflection, with a Philips X'PERT MPD X-ray diffractometer (PANalytical, Royston, UK) operating at 40 kV and 40 mA, in the range of $2\theta = 10\text{-}80°$, at a scanning rate of 0.01°/s with a step size of 005°, equipped with a Cu sealed tube using Kα radiation ($\lambda = 1.54056$ Å). The data were analyzed using Pert Quantify software.

Sample density was evaluated according to the eq. 3:

$$\rho^S = \frac{m}{A*\lambda} \quad (3)$$

where A is the sample area (cm^2), λ the sample thickness (cm), m the sample dry mass (g) and ρ^s the dry matter density of the sample (g/cm^3) [41]. The determination of dry mass value was carried out after removing the water content inside the sample using a vacuum pump for 24 h and then conditioning the sample in a desiccator for 7 days. The sample density was expressed as the average of five measurements.

Thermogravimetric analysis (TGA) was carried out in oxidative atmosphere with a Mettler TC-10 thermobalance from 25 to 800 °C, at a heating rate of 10 °C/min.

Sorption isotherms of water vapor were estimated using a DVS Automated multi-vapor gravimetric sorption analyzer, using N_2 as a carrier gas. Samples (10 mg) were exposed to increasing water vapor pressures obtaining different water activities $a_w = P/P_0$ (from $a_w = 0.05$ to $a_w = 0.8$, T = 30 °C), where P is the partial pressure and P_0 is the saturation water pressure. The adsorbed water amount was measured by a microbalance and recorded along the time (C_{eq} ($g_{solvent}/g_{dry\ basis}$)). In order to analyze the sorption isotherms, the Ferro Fontan model (eq. 4) was adopted [42–44]:

$$M = \left[\frac{\gamma}{\ln\left(\frac{\alpha}{a_w}\right)}\right]^{\frac{1}{r}} \quad (4)$$

where M is the equilibrium moisture content (on dry basis), γ is a parameter accounting for the structure of sorbed water while α and r are parameters to be determined.

The sorption parameters have been evaluated, considering Henry's law of solubility (eq. 5):

$$S = \frac{dc_{eq}}{dP} \quad (5)$$

The no-linear behaviour of diffusion coefficients was modelled through a semi-empirical relation (eq. 6):

$$D = A + \alpha^{*}\mathrm{erf}(\beta^{*}c) + \gamma c \quad (6)$$

where erf is the function error and A, α, β, γ are parameters to be estimated. To facilitate the numerical calculations, an approximated form of eq. 6 was used (eq. 7) [45]:

$$D = A + \frac{2\alpha}{\sqrt{\pi}}*\sqrt{1-e^{-(\beta^{*}c)^2}}*\left(\frac{\sqrt{\pi}}{2} + \frac{31}{200}e^{-(\beta^{*}c)^2} - \frac{341}{8000}*e^{-2*(\beta^{*}c)^2}\right) + \gamma c \quad (7)$$

Zimm-Lundberg theory was applied to evaluate the water clustering degree [46]. The free energy function can be estimated as the first derivative of activity evaluated upon the volume fraction [47]. So, the mean cluster size (MCS) is evaluated from eq. 8:

$$MCS = 1 + \frac{\varnothing^{*}G_s}{V_s} \quad (8)$$

where G_s is the cluster integral v_s is the partial molar volume of penetrant, Ø is the volume fraction of penetrant. The MCS, representing an estimation of cluster size, is evaluated from isotherm sorption curves through the following eq. 9:

$$MCS = (1-\varnothing)^{*}\frac{a_w}{\varnothing}\left(\frac{\partial\varnothing}{\partial a_w}\right)_{p,T} \quad (9)$$

Considering the Ferro-Fontan model equation, MCS could be evaluated through the following relation (eq. 10):

$$MCS = \frac{1}{r}*\frac{a_w}{C_{eq}}*\frac{a^{\frac{1}{r}}*\left(\frac{1}{\ln\frac{\gamma}{a_w}}\right)^{\frac{1}{r}+1}}{\left[1 + a^{\frac{1}{r}}*\frac{\rho_s}{\rho_w}*\left(\frac{1}{\ln\left(\frac{\gamma}{a_w}\right)}\right)^{\frac{1}{r}}\right]^2} \quad (10)$$

where ρ_w is the water density at the experimental temperature while ρ_s is the polymer density evaluated according to ASTM D792.

The acid-base potentiometric titration curves in salt concentration (NaCl 0.1 M) were used to measure the proton adsorption or proton charge. An aliquot of aqueous suspension (40 mL) containing 0.2 g of sample was equilibrated for 30 min until equilibrium pH was reached. The titration started with the addition of NaOH; the pH rapidly reached a constant value. The titration was carried out using HCl solution (1 M) and stopped when the pH was roughly 2.5. The proton adsorption or proton surface charge density σ_H (mol/m^2) determined from potentiometric titration was calculated as the difference between total amounts of H^+ added to the dispersion and that were required to bring a blank solution of the same NaCl concentration to the same pH [48] (eq. 11)

$$\sigma_H = \frac{V}{m^{*}S}*\left\{\left([H^+]_b - [H^+]_s\right) - \left(\frac{K_w}{[H^+]_b} - \frac{K_w}{[H^+]_s}\right)\right\} \quad (11)$$

Where V is the volume of electrolyte solution (0.04 L), m is the sample mass, S is the specific surface area, $[H^+]$ is the solution proton concentration (mol/L), subscripts b and s refer to blank and sample solutions while K_w is the dissociation product of water ($1*10^{-14}$). The surface area of tested samples was evaluated by means of BET isotherm. Moreover, since the sorption data follow the type III isotherm, typical BET model cannot be directly applied and a corrective model should be applied. The methodology proposed by Taguchi et al. allows to estimate the monolayer capacity of systems following the type III isotherm [49] by evaluating a specific water activity a_w* through eq. 12:

$$a_w^{*} = \frac{-1 \pm C_{max}^{0.5}}{C_{max}^{-1}} \quad (12)$$

where C_{max} is the C constant evaluated by applying BET model for low water activities ($a_w < 0.4$). Afterwards, the theoretical monolayer capacity w_m was estimated by finding the y value which corresponds to $x = a_w$*. So, the specific area was calculated through eq. 13:

$$S_{bet} = \frac{w_m{}^{*}N_a{}^{*}A}{\rho_w} \quad (13)$$

where N_a is the Avogadro number, A is the mean water molecules area ($10.8*10^{-20}$ m^2) and ρ_w is the water density.

The light-radiation transmission spectra (T %) were investigated using Spectrometer UV-2401 PC Shimadzu (Japan) in the range of 280–500 nm. Transmission spectra were reported as function of wavelength (nm). The Ultraviolet Protection Factor (UPF) was evaluated according to AATCC Test Method 183–2004 Transmittance or Blocking of Erythemally Weighted Ultraviolet Radiation through Fabrics. For each specimen, UFP was evaluated according to eq. 14:

$$UFP = \frac{\sum_{280\,nm}^{400\,nm} E_\lambda{}^{*}S_\lambda{}^{*}\Delta\lambda}{\sum_{280\,nm}^{400\,nm} E_\lambda{}^{*}S_\lambda{}^{*}T_\lambda{}^{*}\Delta\lambda} \quad (14)$$

where:

E_λ = relative erythemal spectral effectiveness.

S_λ = solar spectral irradiance.

T_λ = average spectral transmittance of the specimen.

$\Delta\lambda$ = measured wavelength interval (nm).

The percent blocking for UV-A and for UV-B was evaluated by using eq. 15 and eq.16:

$$\%\,\mathrm{Blocking\,UV-B} = 100\% - \frac{\sum_{280\,nm}^{315\,nm} T_\lambda{}^{*}\Delta\lambda}{\sum_{280\,nm}^{315\,nm}\Delta\lambda} \quad (15)$$

$$\%\,\mathrm{Blocking\,UV-A} = 100\% - \frac{\sum_{315\,nm}^{400\,nm} T_\lambda{}^{*}\Delta\lambda}{\sum_{315\,nm}^{400\,nm}\Delta\lambda} \quad (16)$$

A QUV accelerated weathering tester by Q-Panel (LAB PRODUCTS) was used to perform the weathering test. The radiation spectrum centered in the ultraviolet wavelengths was supplied by a fluorescent UV lamps with a wavelength of 340 nm and the irradiance level of 0.78 W/m^2. The temperature in the chamber was fixed at 45 °C while the moisture level was 50 %. The produced samples were adequately mounted in the sample holder in the chamber. The samples were exposed for 45 days. The mounted films were withdrawn from the device at different times and analyzed using FT-IR.

Fourier Transform Infrared spectra of the samples were collected by a Thermo Scientific Nicolet 600 FT-IR, equipped with a Smart Performer accessory for attenuated total-reflection (ATR) measurement. The operating spectral range was set at 650–4,000 cm^{-1}, with a resolution of 4 cm^{-1}and 64 scans per sample.

Color difference (ΔE) values were measured using a ColorimeterX software. The color difference calculation was performed based on CIE L*a*b color difference equation [50] (eq. 17):

$$\Delta E^{*} = \sqrt{\left(L_2^{*} - L_1^{*}\right)^2 + \left(a_2^{*} - a_1^{*}\right)^2 + \left(b_2^{*} - b_1^{*}\right)^2} \quad (17)$$

L* characterizes the grey value and it ranges between 100 (white) and 0 (black), while a* and b* are the chromaticity coordinates. The subscript 1 refers to the state before UV exposure, while subscript 2 denotes the state after UV exposure. The (a_2* − a_1*) positive values

describe a red shift; the ($a_2^* - a_1^*$) negative values describe the green shift, ($b_2^* - b_1^*$) positive values characterize the yellow shift, while ($b_2^* - b_1^*$) negative values refer to the blue shift [36]. Each sample was measured four times and the data are reported as mean and standard deviation.

Liquid retention of electrospun fabric were performed by immersing a pre-weighed mass of sample (previously dried for 8 h under vacuum at 50 °C and weighed (M_0)) in 25 mL of different liquid solutions (pure water, lemon juice (pH = 3), NaOH solution (pH = 13) and sweat simulant (pH = 5.5)). Sweat simulant was prepared according to EN 1811:2011 by dissolving NaCl (10.8 g), lactic acid (1.2 g), urea (1.3 g) in 1 L of distillate water. pH was adjusted to 5.5 by dropping NaOH solution. Liquid retention tests were performed at 37 °C for 1 h. After that, the samples were pressed using a pneumatic press for 10 s applying a pressure of 1 ton to remove any excess of solvent and re-weighed (M_{eq}). The retention degree was evaluated according to the eq. 18:

$$q\left(\frac{g}{g(d.b.)}\right) = \frac{M_0 - M_{eq}}{M_0} \quad (18)$$

2.3.2. Microbiological assays and bacterial strains

The antimicrobial activity of the films was estimated by determining the inhibitory effects of PU@Cu, PU@Zn and PU@Cu/Zn samples on bacterial growth at 16, 20 and 24 h and comparing with the control sample (PU), the same material without metal. All the growths were in Luria-Bertani (LB) broth (tryptone, 10 g/L; yeast extract 10 g/L; sodium chloride, 5 g/L, pH = 7). Briefly, bacteria from an 18 h pre-inoculated culture were suspended in fresh medium at density of 5×10^5 CFU (colony forming unity)/mL and incubated at 37° C in the presence of 1.5 cm^2 of each film, divided into four pieces, with constant shaking (250 rpm). At the times indicated, the effects on growth were evaluated by turbidity, measuring the optical density (OD) at 600 nm. For each sample the results were reported as the mean of three independent experiments, each in triplicate, and expressed as a percentage of the ratio to those of the controls at the corresponding times. The inhibitory effect was estimated by subtracting the single percentage values from 100, the percentage value of the controls for each time considered. Antimicrobial activity "A" was also estimated using the following relationship:

A = F – G, with F = (Log C_t − Log C_{t0}) and G = (Log T_t − Log T_{t0}), where C_t and T_t are the optical density detected at the different times t, for control substrate and coated samples, respectively, and C_{t0} and T_{t0} are the respective OD at the initial time t = 0. Bacteria used for microbiological assays were *Escherichia coli* (strain JM109) and the pathogenic *Staphylococcus aureus* (hospital isolate), representative of Gram$^-$ and Gram$^+$, respectively. *E. coli* was purchased from Promega (Madison, Wisconsin, USA). The *S. aureus* strain was obtained from the microbial collection deposited in the microbiology laboratory of the Department of Chemistry and Biology of University of Salerno [51].

2.4. Statistical analysis

The statistical significance of the obtained data was assessed by performing a one-way ANOVA test. Tukey's post hoc method was carried out for assessing significant differences between means ($p < 0.05$). The statistical comparisons were obtained by means of the Statistix software.

3. Results and discussion

3.1. Properties of PU based fiber membrane

The samples microstructure of PU based fiber membranes was investigated by SEM (Fig. 1).

Fig. 1a reports the SEM micrograph of bare PU electrospun fibers. Inset shows a higher magnification (5200x) of the same sample. The

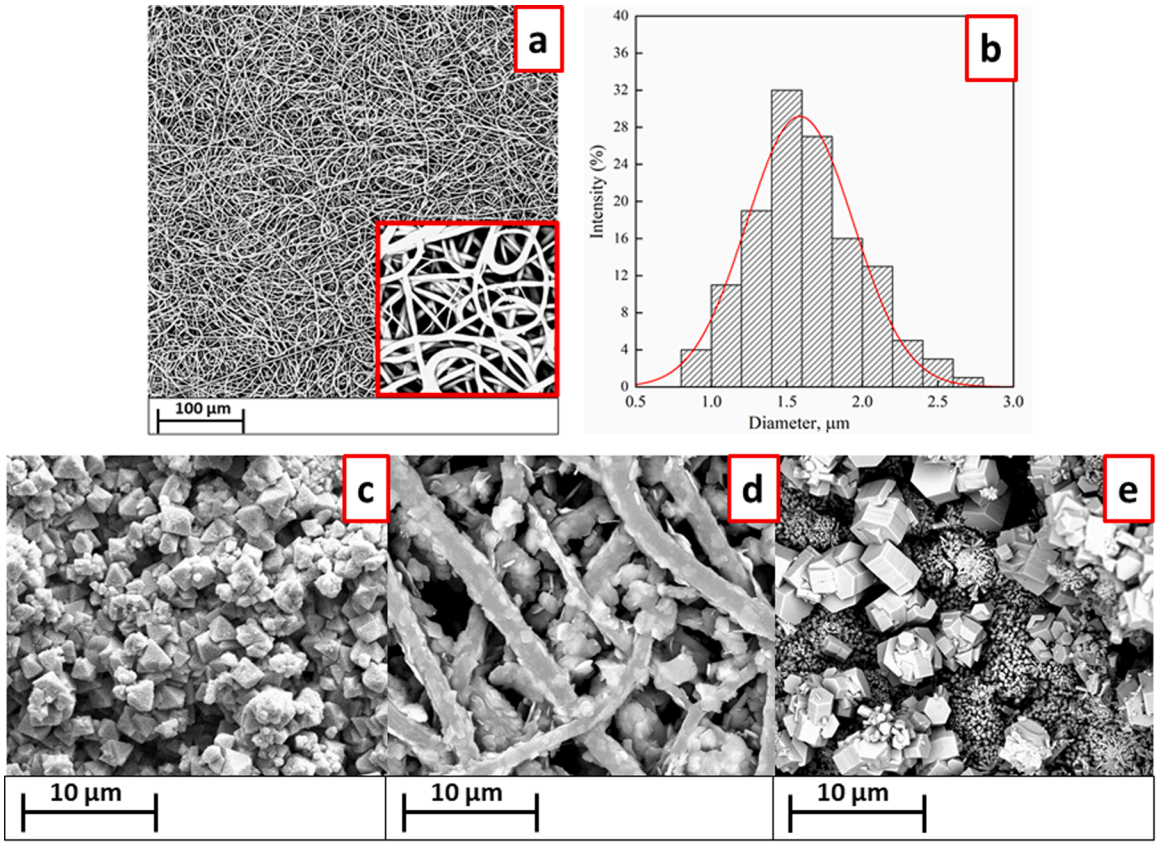

Fig. 1. SEM micrographs of a) PU; b) diameter distributions of PU fibers; c) PU@Cu; d) PU@Zn and e) PU@Cu/Zn.

electrospun structure appears as an interconnected network without defects and beads-free with a mean diameter of roughly 1.58 ± 0.22 μm (Fig. 1b). Fig. 1c reports the electrospun PU@Cu where octahedral like structures have been formed after copper salt precipitation. Fig. 1d shows zinc modified PU sample where platelets like aggregates are evident since the formation of zinc-based structures while Fig. 1e shows the SEM image of Cu/Zn PU modified fibers which clearly puts in evidence the prismatic like structured of copper and nanorods of zinc. As far as the modified PU membrane with copper and copper/zinc, the fibrillar morphology cannot be clearly visible anymore. The in-situ growth of metal-oxide structures is an acid − base neutralization. It can be considered that the precursors provided the transition-metal ions and reacted with the bases (such as NH_4OH) as the Lewis acid. The aqueous solution of precursors was neutralized by the base (NH_4OH) producing their corresponding metal oxides, according to the following reactions [52]:

$$M^{2+}_{(aq)} + 2OH^{-}_{(aq)} \rightarrow M(OH)_2\downarrow$$

$$M(OH)_2 \rightarrow MO\downarrow + H_2O$$

where M represents transition-metal element. EDX-SEM maps (Fig. 2) report the copper (green areas) and zinc (blue areas) distribution on PU fibers for the three different samples with a weight ratio of Cu/Zn of 2.6 for PU@Cu/Zn. Then, it can be observed a good and homogeneous deposition of the two elements. Insets in the left corner (Fig. 2 a-b) report the 3D structures of CuO and ZnO obtained from Avogadro Software.

The investigation of SEM micrographs even allowed to obtain the profile plots reported as gray value (pixel intensity) vs pixel distance (Fig. 3).

The gray intensity value of the membranes increases from 120 to 190, 87 to 150, 120 to 180 and 100 to 170 for PU, PU@Cu, PU@Zn and PU@Cu/Zn, respectively. In the three-dimensional surface profiles, the topology clearly differs each other in height. Regions with very low pixel intensity values are seen as blue plateau. The R_a and RMS parameters are reported in Table 1 where it is possible to observe a change in profile height deviations after the precipitation of copper-based structures (both parameters decrease) while no statistical differences can be observed for PU@Zn systems. The 3-D maps in Fig. 3 confirmed the trend of the parameters reported in Table 1.

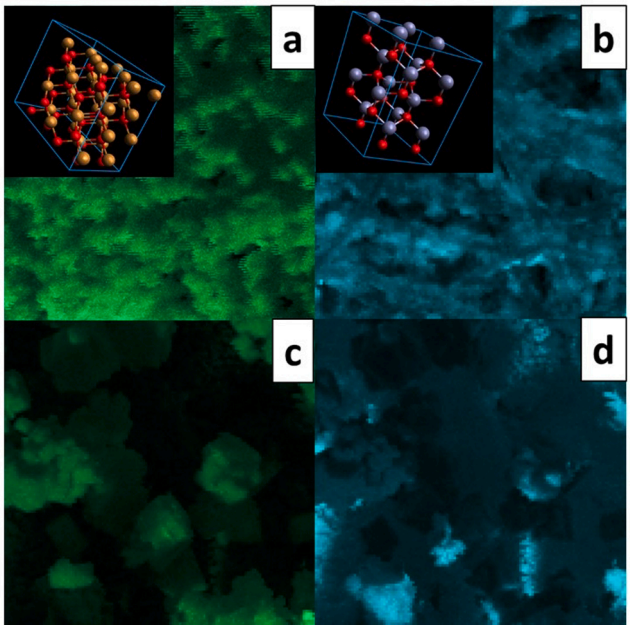

Fig. 2. Element color mapping of PU@Cu (a); PU@Zn (b) and PU@Cu/Zn (c (Cu) and d (Zn)).

Fig. 4a reports the XRD spectra of PU and modified PU based samples.

As far as PU sample concerns, a broad peak, characteristic of amorphous system, is centred at about 22° of 2θ [53]. In the PU@Zn spectrum, apart from PU broad peak, characteristic crystalline peaks of zinc oxide in wurtzite form can be detected. The main ones are centred at 2θ = 31.84°, 34.42°, 36.33°, 47.63°, 56.71°, 62.96°, 68.13°, and 69.18° whom Miller indexes are reported above the related peaks [54]. The spectrum of PU@Cu shows tight crystalline peaks of CuO and Cu_2O (◆) [55]. Some characteristic peaks of copper hydroxide are even evident (♣). Finally, XRD spectrum of PU@Cu/Zn clearly shows the characteristic peaks belonging to copper and zinc. Fig. 4b reports the surface charge density of different samples obtained from titration experiments. At pH values below the point of zero charge (PZC), the chemical groups on the particle surface are essentially protonated resulting in possessing a positively charged surface while, above it, the groups are deprotonated showing a negatively charged surface. The neat PU shows a PZC of 5.80 while it changes for PU@Cu/Zn (6.90), PU@Cu (3.21) and PU@Zn (4.21). These latters could be ascribed to the electronegativity of copper and zinc elements. In literature, many empirical models have been reported to describe the relationship between electronegativity and PZC showing an inverse dependence between them (a higher value of electronegativity determines a lower value of PZC).

Fig. 5 reports the thermogravimetric curves of PU and surface modified PU electrospun fibers.

The thermal degradation can be regarded as a complex process since it involves several decomposition reactions caused by random chain scission [56]. At low temperatures (T < 150 °C) loss of water was observed. The main degradation step (250 °C < T < 350 °C) is associated to the decomposition of the hard segment due to the breakage of polyurethane bond forming di-isocyanates, diols and CO_2 [57,58]. The second step (350 °C-420 °C) is due to the decomposition and scission of the soft segments [58,59]. The third step at high temperatures (420 °C-600 °C) concerns the oxidation process of the carbonaceous residue formed in the previous steps. The PU modified samples showed a reduction of water loss rising from adsorbed water and crystal water [60] while a slight shift of the main thermal decomposition step occurred. In the same thermal range, dehydroxylation could even happen. The residue amount is noticeably higher than neat PU (21 % for PU@Cu, 7 % for PU@Zn and 66 % for PU@Cu/Zn). Such improvement could be attributed to higher stability of copper and zinc complexes as well as to the fact that the transmission of oxygen and other gaseous product is hindered by inorganic coating which could slow down further thermal breakdown, being a barrier between the heat source and the material.

Fig. 6 shows the sorption isotherms of neat PU and PU fiber membrane, reporting the equilibrium moisture content (on dry basis) as a function of the water activity.

Sorption isotherms follow the typical type III isotherm according to BET classification [61]. All the curves showed the same behavior in the entire a_w range. For low activity, no noticeable differences are evident. As activity increases, the plasticizing effect of water and the increase in segmental motion contribute to increase the adsorbed moisture adsorbed. In fact, for high a_w, it can be observed a reduction of adsorbed water content for PU@Cu and PU@Cu/Zn. Probably, this effect could be correlated to the low availability of accessible polar sites. Meanwhile, the zinc covered PU sample showed a slight increase in water adsorption. The phenomenon, being of thermodynamic nature, can be related to the variation of active sites on the surface of PU electrospun fibers. The modeling of sorption data has been carried out using Ferro-Fontan equation. The extrapolated parameters are reported in Table 2.

The experimental data of diffusivity show to follow similar trend (pseudo-parabolic) with an initial increase in diffusion followed by a decrease as a_w increases. The reduction of diffusion for PU@Cu and PU@Zn could be ascribed to the presence of inorganic structures which

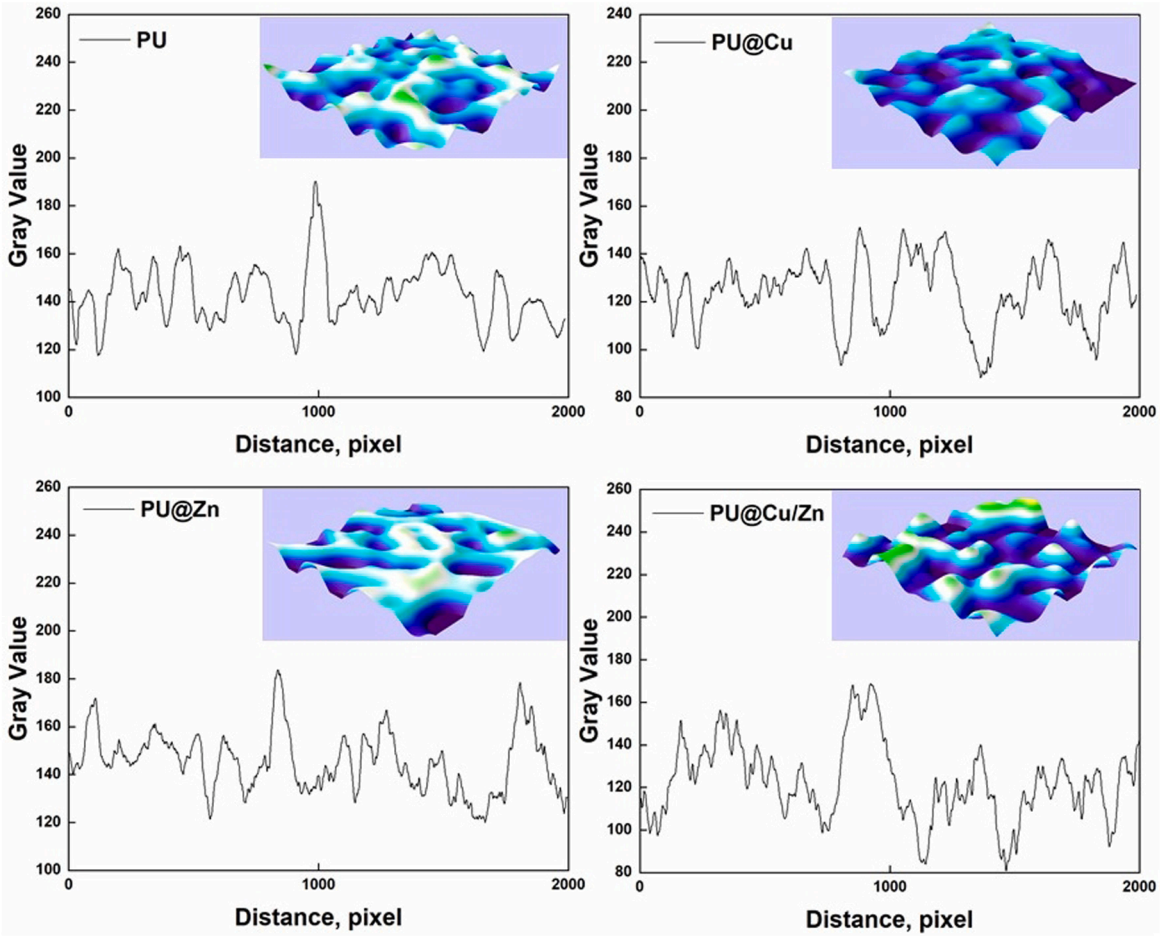

Fig. 3. Profile plots and 3D surface plots of electrospun systems.

Table 1
Ra and RMS parameters.

Sample	R_a	RMS
PU	142.5 ± 1.2^a	143 ± 1.4^a
PU@Cu	123.2 ± 0.9^b	124.1 ± 0.8^b
PU@Zn	143.5 ± 1.3^a	144.1 ± 1.1^a
PU@Cu/Zn	120.2 ± 1.1^c	121.43 ± 0.9^b

For each fiber membrane, different superscript letters in the same column indicate that the mean values are significantly different ($p \leq 0.05$).

can constitute a physical barrier able to increase the tortuosity of the system and, so, the pathway of water molecules. Besides, after the deposition, the average porosity is supposed to be reduced (as SEM images proved) further leading to a reduction of diffusion coefficients [62]. The fitting of diffusion data reported in Fig. 6b allowed to extrapolate the parameters of equation 7 which were reported in Table 3.

The mean diffusion was estimated through a mathematical evaluation by applying eq. 19:

$$D_{media} = \frac{1}{\Delta C_{eq}} \int_{c_i}^{c_f} D(c)\, dc \qquad (19)$$

Sorption coefficient, mean diffusion coefficient and permeability are reported in Table 4.

Fig. 7 reports the liquid retention tests of PU and modified PU by testing four different liquid media.

The observed trend cannot be simply described since many overlapped factors affect the retained amount such as roughness, porosity, polar surface sites and point of zero charge. Concerning the water retention test, the pristine PU is able to retain a higher amount of water while a lower retention degree was observed for modified electrospun membranes, probably due to the reduction of porosity and roughness ascribed to the metal oxide formation. This trend can be correlated to the higher porosity of pristine PU systems allowing water to better go through it. The higher porosity and roughness of PU@Zn compared to PU@Cu is responsible for an augmented retained water amount while PU@Cu/Zn appears to possess an intermediate behavior compared to PU@Cu and PU@Zn systems. Concerning the retention of sweat simulant, it is needed to consider the point of zero charge of electrospun systems. PU and PU@Cu/Zn possess a PZC > pH of medium; so, a negative charge onto the surface is present leading to the formation of weak electrostatic interactions with cationic groups. Besides, PU@Cu and PU@Zn possess a PZC < pH of sweat simulant so a net positive charge is present and responsible for weak interactions with anionic groups such as chloride anion and lactate ion. In basic conditions, it is known that weak interactions can exist between amino groups of near urethane chains leading to the formation of an interconnected network [63]. This phenomenon can weigh on reduction of free volume. Finally, in acidic medium, the protonation of amino groups can lead to a swelling of polymeric system favouring the entry of water molecules.

3.2. Evaluation of UV-stability

The UPF measurements were carried out in the range 280–500 nm. Fig. 8 shows the transmittance versus wavelength for all the specimens.

It firstly was investigated the effect of morphology on transmission. A PU film made by compression molding (CM) was produced by pressing

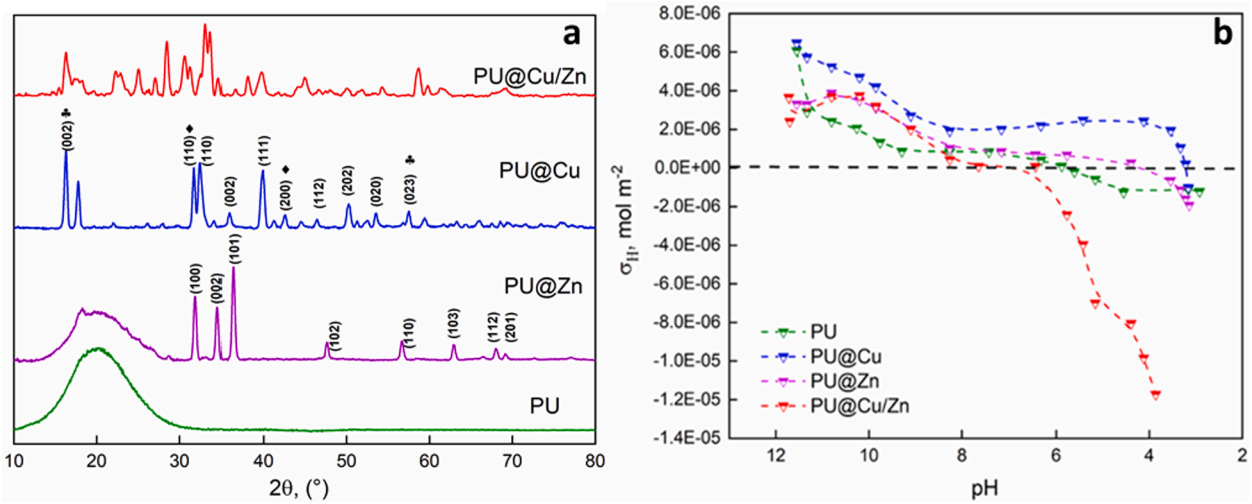

Fig. 4. XRD spectra of PU based electrospun membranes; b) Surface charge vs pH for PU and modified PU.

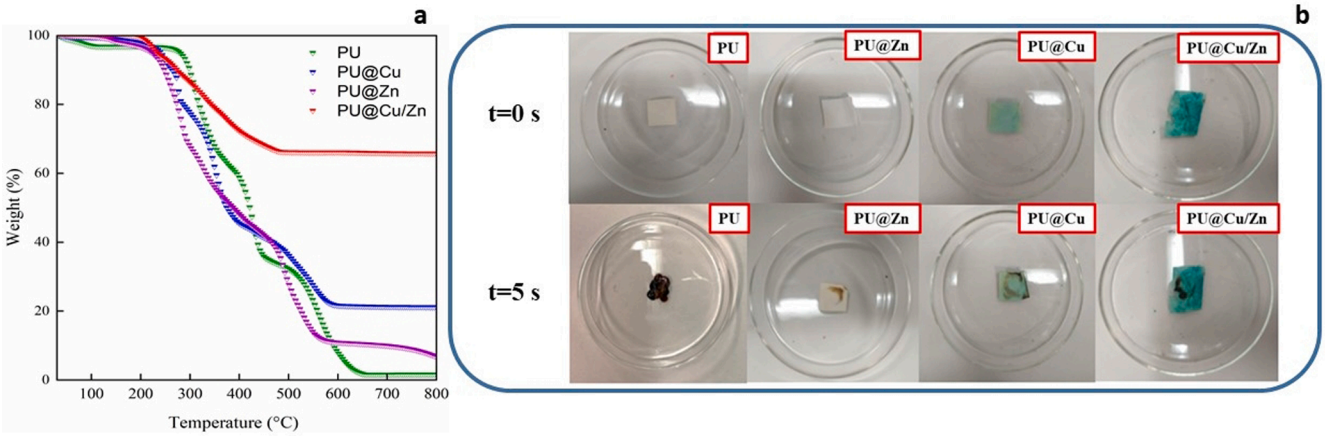

Fig. 5. TGA curves of PU and modified PU fiber membrane (a) and pictures of flame contact test (b).

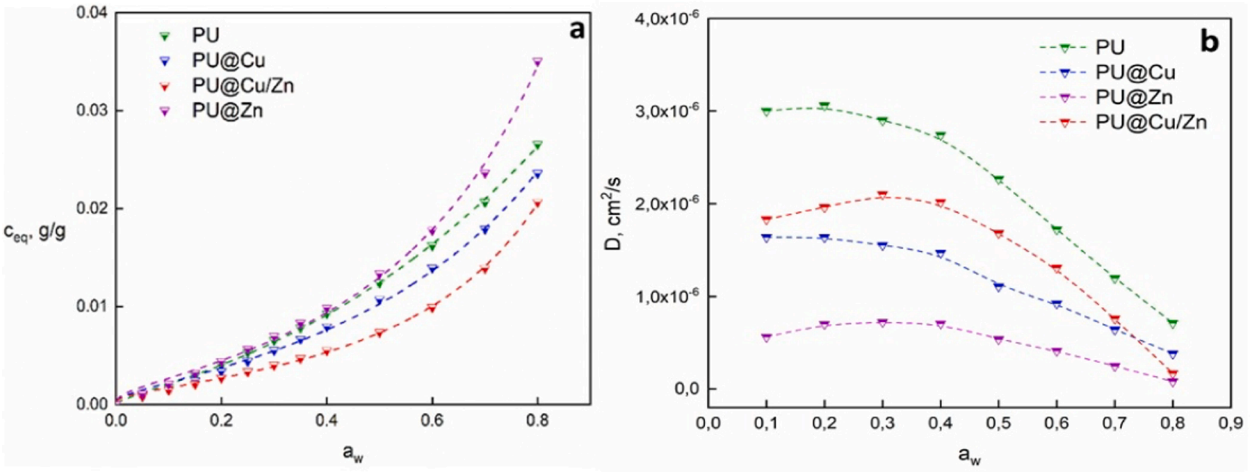

Fig. 6. a) sorption isotherms and b) diffusion coefficients versus a_w for PU and PU fiber membrane.

PU pellets at 120 °C for 1 min applying a pressure of 1 ton. It was clear that the micrometric dimensions of electrospun fibers led to a noticeable reduction (about 99.8 %) of transmission along the wavelength range. This effect could be attributed to the light scattering phenomenon due to the interconnected network of PU electrospun system. Then, the effect of surface modification with Cu and Zn was investigated. In all cases, a reduction of T% was achieved after the modification and this effect was clearly visible for Cu covered PU membranes. It is then worthwhile

Table 2
Ferro-Fontan parameters obtained from fitting of experimental data.

Sample	r	γ	α
PU	0.276 ± 0.02^{c}	6.193 ± 0.25^{a}	0.750 ± 0.03^{a}
PU@Cu	0.520 ± 0.04^{b}	1.888 ± 0.18^{b}	0.123 ± 0.09^{b}
PU@Zn	0.573 ± 0.05^{b}	1.493 ± 0.16^{bc}	0.091 ± 0.01^{b}
PU@Cu/Zn	0.690 ± 0.04^{a}	1.249 ± 0.11^{c}	0.030 ± 0.008^{b}

For each fiber membrane, different superscript letters in the same column indicate that the mean values are significantly different ($p \leq 0.05$).

Table 3
Parameters extrapolated from equation 7.

Samples	A [10^{-6} cm^2 s^{-1}]	α [10^{-6} cm^2 s^{-1}]	γ [10^{-6} cm^2 L s^{-1} mol^{-1}]	β [L/mol]
PU	2.5 ± 0.1^{c}	1.2 ± 0.1^{b}	-115 ± 3^{b}	350 ± 12^{a}
PU@Cu	4.2 ± 0.2^{b}	2.2 ± 0.1^{c}	-6 ± 1^{c}	4 ± 1^{c}
PU@Zn	3.1 ± 0.1^{c}	0.1 ± 0.01^{d}	-2 ± 0.1^{c}	3 ± 0.2^{c}
PU@Cu/Zn	1.4 ± 0.4^{a}	0.6 ± 0.2^{a}	-109 ± 4^{a}	505 ± 8^{b}

For each fiber membrane, different superscript letters in the same column indicate that the mean values are significantly different ($p \leq 0.05$).

Table 4
Sorption, diffusion and permeability of PU and PU fiber membrane.

Sample	Sorption coefficient [g g_{db}^{-1} atm^{-1}]	Mean diffusion 10^6 [cm^2 s^{-1}]	Permeability 10^6 [g g_{db}^{-1} atm^{-1} cm^2 s^{-1}]
PU	0.51 ± 0.08^{ab}	2.21 ± 0.12^{a}	1.12 ± 0.10^{a}
PU@Cu	0.45 ± 0.05^{ab}	0.98 ± 0.13^{b}	0.44 ± 0.11^{b}
PU@Zn	0.57 ± 0.11^{a}	0.41 ± 0.02^{c}	0.23 ± 0.01^{b}
PU@Cu/Zn	0.31 ± 0.05^{b}	1.16 ± 0.15^{b}	0.37 ± 0.07^{b}

For each fiber membrane, different superscript letters in the same column indicate that the mean values are significantly different ($p \leq 0.05$).

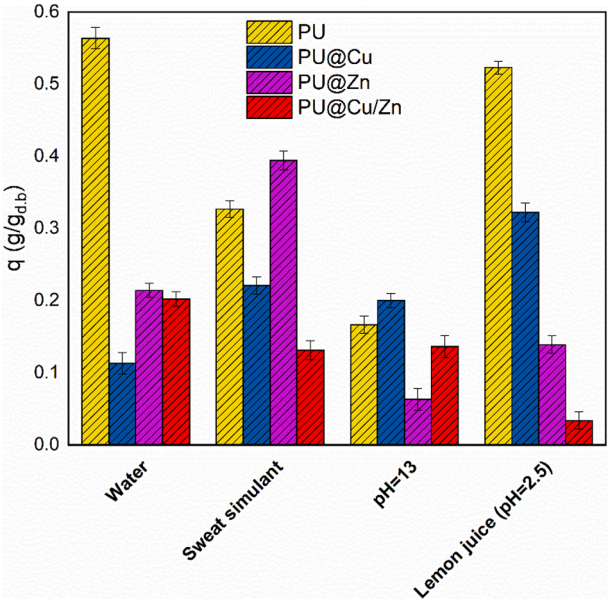

Fig. 7. Liquid retention of PU and modified PU.

noticing that a 0 % transmission was achieved for PU@Cu/Zn sample. Applying the relations reported previously, the ultraviolet protection factors as well as the UV-A and UV-B protection factors were estimated. The obtained data are reported in Table 5.

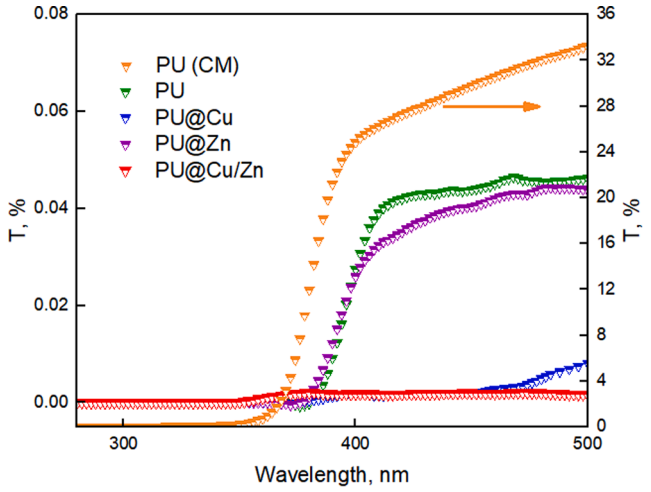

Fig. 8. Transmittance spectra of PU based samples.

Table 5
UPFs, UV-A and UV-B blocking factors.

Sample	UPF	% blocking UV-A	% blocking UV-B
PU	50+	99.997	100
PU@Cu	50+	99.999	100
PU@Zn	50+	99.996	100
PU@Cu/Zn	50+	99.999	100
PU (CM)	2.84	93.923	99.996

The noticeable differences involving the UPFs of PU and PU (CM) justified and corroborated the previously reported statements while slight differences of % blocking of UV-A and UV-B are evident.

Additionally, the PU modified samples displayed better light shielding effect than the uncoated PU in the whole wavelength range, mainly because of its stronger absorption and scattering owing to their special structures. In fact, the use of materials with UV-protection properties is typically based on optical scattering and/or absorption. This effect could be attributed to the strong UV-absorption of the hierarchical microstructures (octahedral structures, sheet-like structure of Zn and prismatic and rods for Cu/Zn). Then, light scattering and light reflection of the porous structures contributed to improve the ultraviolet blocking performances of PU. Besides, the surface roughness increased after the modification leading to higher UV reflection and preventing the penetration of UV-rays.

The preservation of surface characteristics is important for aesthetic reasons, so the presence of a light stabilizer is an important issue and the evaluation of UV stability is fundamental. Accelerated weathering tests were carried out to evaluate the stability of the membrane along time. Fig. 9 shows FTIR spectra concerning the C═O band in the range 1700–1730 cm^{-1} as function of exposure time. The peak at 1730 cm^{-1} characterizes C═O stretching vibrations in ester structure while the peak at 1705 cm^{-1} corresponds to C═O stretching vibration in the urethane bond [36]. The aromatic structures of PU are known to be not stable to light and susceptible to rapid degradation during UV exposure.

Fig. 9 shows an initial (1 day) decrease in C═O band intensity while, as exposing time increases, an increase in band intensity is evident especially for pristine PU membrane which is responsible for the yellowing of electrospun membrane. This no linear trend of carbonyl peak intensity could be ascribed to different reactions such as Norrish type I, which implies a reduction of carbonyl groups and Photo-Fries mechanism correlated to the increase in C═O intensity [64]. To better investigate the effect of UV degradation on PU systems it is necessary to study the photo degradation mechanism of aliphatic and aromatic groups. The photodegradation mechanisms for aliphatic and aromatic PUs are

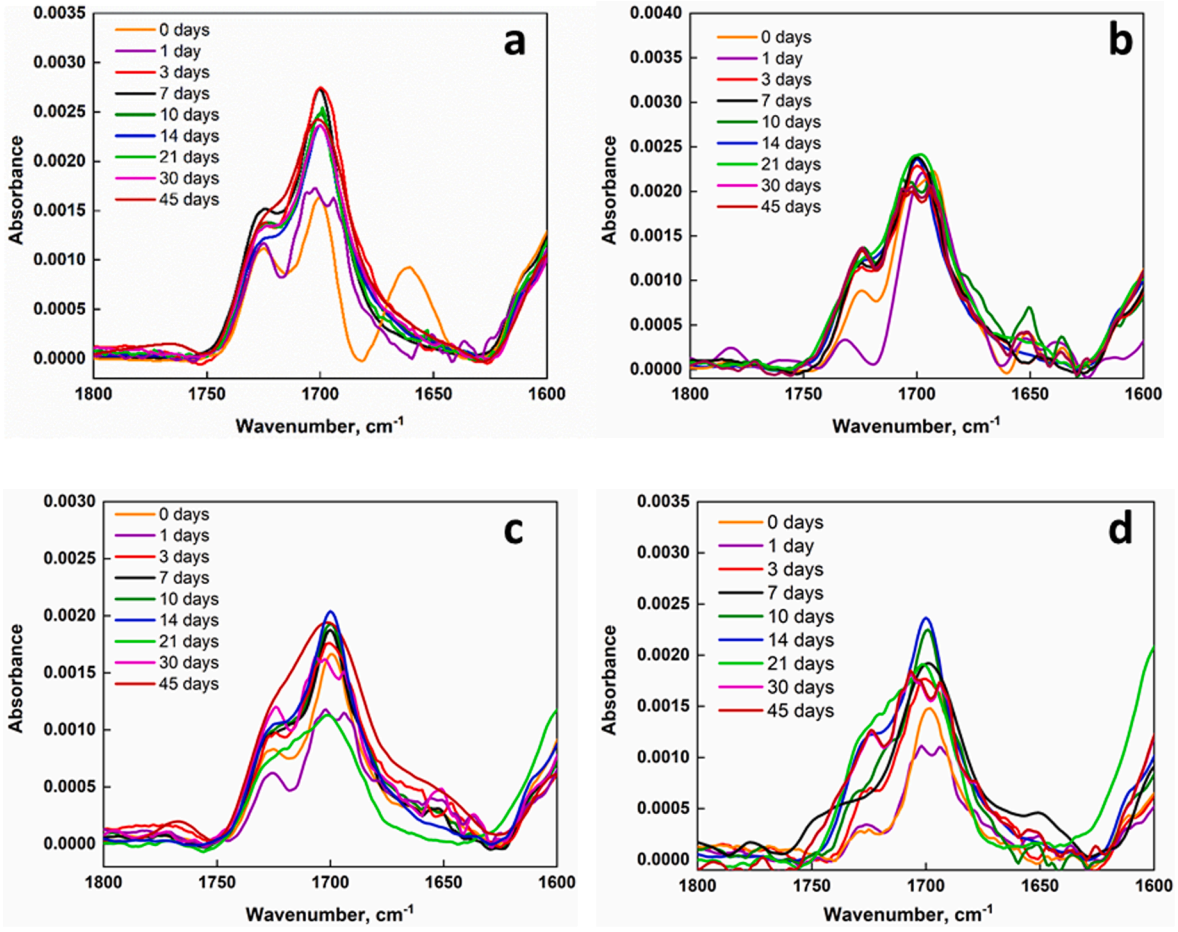

Fig. 9. C═O band intensity of PU (a), PU@Zn (b), PU@Cu (c) and PU@Cu/Zn (d).

different. Firstly, chain scissions are verified since the Norrish type I reaction (Scheme 1). The photolytic reaction induced the formation of free radicals able to extract hydrogen from CH_2 groups leading to the generation of a polymer peroxy radicals (PO_2•) and hydroperoxides (POOH). The UV induced cleavage of polymer hydroperoxides can form polymer oxy radical (PO•) through β-scission reactions as well as by forming POH due to the hydrogen extraction. These two reactions can generate alkyl radicals. The termination steps occurred via reaction involving different radicals causing crosslinking (Scheme 1) [64,65].

In parallel, the degradation mechanism of aromatic group is quite complex and mainly involve two kinds of mechanisms: Photo-Fries reaction with formation of quinone imide and diquinone imide and Norrish type I (Scheme 2).

The photodegradation mechanism of aromatic groups is known to be quite complex. Aromatic diisocyanates are supposed to be quite unstable with respect to light [66]. In particular, the degradation can be schematized as follows. The Photo-Fries rearrangement of phenyl groups can occur during irradiation. At high wavelength, the aromatic structures were oxidized in the central methylene group, leading to highly conjugated quinone imide generated from phenyl groups. The formed quinoid structures are the main cause of yellowing, being a strong chromophore [36,67]. The change in color can be correlated to the increase in carbonyl groups. Moreover, the further irradiation can induce random chain scissions by Norrish type I. However, at low wavelength, photo induced oxidation of aromatic PUs might occur.

Carbonyl Index (CI) is a parameter able to estimate the resistance to photodegradation. It is easily calculated through the equation 20:

$$CI = \frac{\int Abs_{1850-1650\ cm^{-1}}}{\int Abs_{1500-1420\ cm^{-1}}} \quad (20)$$

The obtained data at each irradiation time are reported in Fig. 10:

It can be observed that the CI tends to increase for all the specimens as the exposure time increases. This is a well-known effect directly linked with the photooxidation of the matrix. This is quite evident for neat PU. After 45 days, the CI is reduced of 54 ± 3 % compared to PU while no noticeable differences are observed for treated samples. The presence of Zn seems to slow down the UV degradation especially for short times while the phenomenon is even observed for PU@Cu/Zn which is demonstrated to be the most promising. The weathering resistance is related to the photooxidation reactions, which occur preferentially close to the surface of the specimen; so, it can be concluded that the use of the metal oxide structures is needed in most cases to ensure their prolonged use. A quick, rough explanation could be that the metal oxides framework slows down the photodegradation rate of the material, resulting in a lower amount of carbonyl groups playing a role in stabilizing PU fibers by acting as screen. The dominant screening mechanism is related to the ability of MO_x to adsorb the UV radiation and hence reduce the UV intensity that can promote the oxidation of the PU chains.

Finally, modelling of C═O trend was proposed. Hypothesizing that the variation of carbonyl concentration along time undergoes to a *n*-power law reaction like, equation 21 can be proposed where k_1 is the rate constant:

$$-\frac{d[CO]}{dt} = k_1 * [CO]^n \quad (21)$$

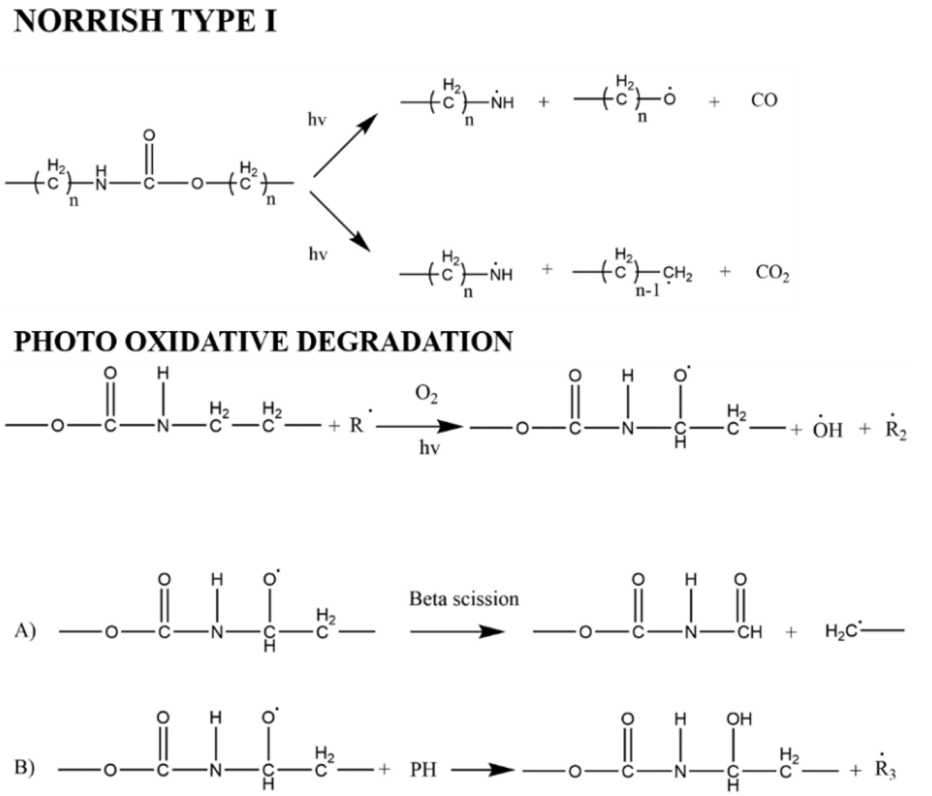

Scheme 1. Photodegradation mechanisms of aliphatic chains.

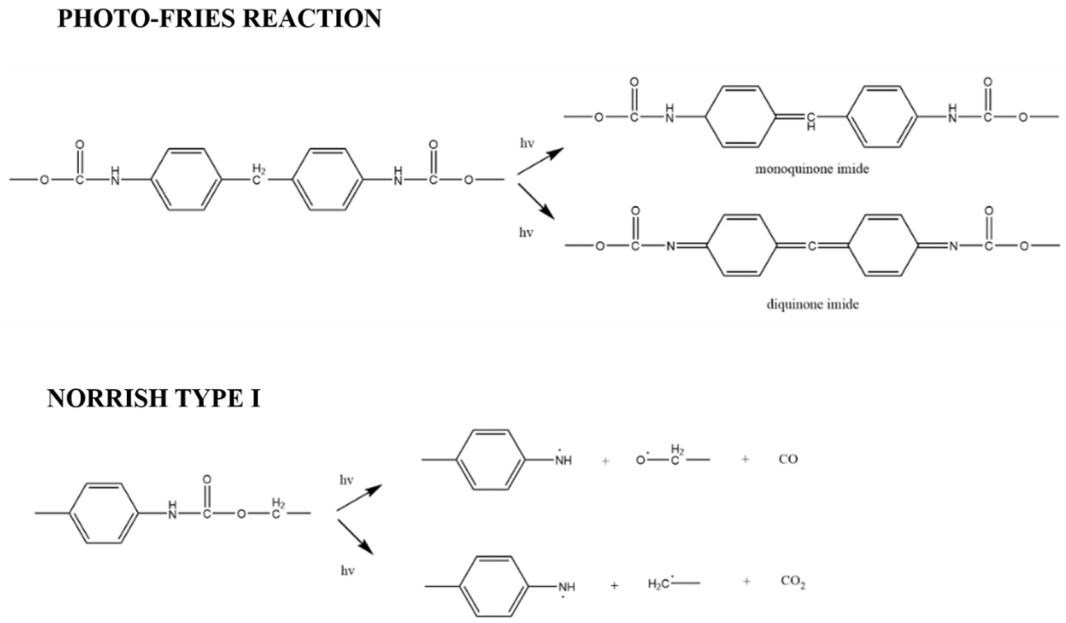

Scheme 2. Photodegradation mechanisms of urethane groups.

By integrating the above reported equation along time and considering that as t approaches to zero [CO] assumes the initial value $[CO]_0$, equation 22 can be derived:

$$[CO] = \sqrt[1-n]{\left\{[CO]_0^{1-n} - (n+1)*k_1*t\right\}} \quad (22)$$

For PU system, assuming the known initial carbonyl concentration $[CO]_0$, it was possible to extrapolate the k_1 and n values (n = -0.127 and $k_1 = 0.22\ d^{-1}$).

For the PU fiber membrane, the carbonyl concentration variation could be described by a similar equation by considering the effect of UV shielding layer (eq. 23):

$$\frac{d[CO]}{dt} = k_1*[CO]^n - k_2*[CO] \quad (23)$$

Where the constant k_2 is related to the presence of UV shielding barrier made of metal oxides. The equation admits the following solution (eq. 24):

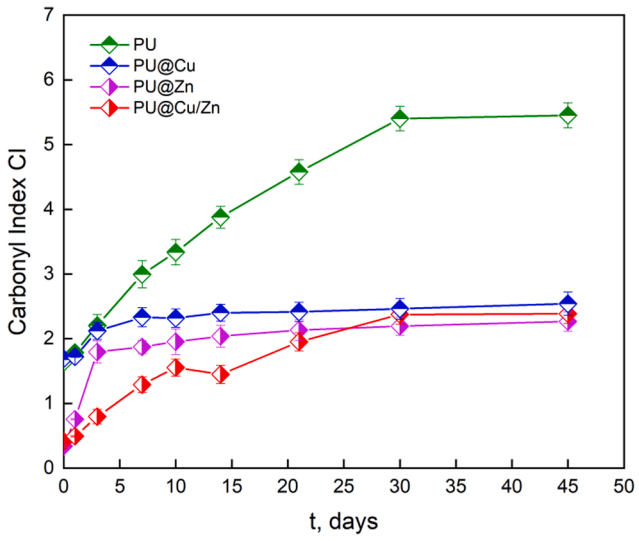

Fig. 10. Carbonyl Index along exposure time.

$$[CO] = \left\{ \frac{k_1 - \left[\left(k_1 - k_2 * [CO]_0^{1-n} \right) * \exp[k_2 * (n-1) * t] \right]}{k_2} \right\}^{\frac{1}{1-n}} \quad (24)$$

The fitting through equation 24 allowed to extrapolate the constant k_2 for each tested system. Values are reported in Table 6.

For PU system, the negative n values let suppose that the reaction rate is inversely proportional with the time-dependent CO concentration. So, as the irradiation time increases, the increase in CO concentration is quite favoured justifying the previously reported data related to the absent screening effect of neat PU system. After the functionalization, the power coefficient became positive and, despite an increase in k_1 values, the quasi similar values of k_2, representative of the shielding effect of metal oxide layer, could noticeably limit the increase in CO concentration due to the UV irradiation. In general, by considering the obtained data, it can be claimed that the presence of copper based structures could favour the UV shielding effect since the high k_2 values respect to PU@Zn system.

To further prove the UV screening effect of the produced materials, chromaticity data were evaluated. The chromaticity analysis was performed to study the colour changes in sample upon UV irradiation. The colour data are presented in Table 7.

It is known that the urethane bridge oxidizes to the quinone-imide structure, the latter being a chromophore, resulting in the yellowing of PU. As the fiber membrane is irradiated, colour shiftings were verified leading to the loss of yellowness (b*) and redness (a*) on the surface. The decrease in a* and b* values are consistent with the reduction in C═O concentration. The lightness (L*), which could be associated to chains scission, tend to decreases with the irradiation since the colour shifts towards yellow. Up to 45 days, the ΔE* values decrease since the reduction of the three chromaticity parameters. Moreover, huge differences could be detected among the samples. The high change in ΔE* value for PU is perfectly in agreement with the previously reported data. These high ΔE values clearly depict the significant yellowing of PU after exposure to UV rays, indicating severe coating deterioration, while it is worthwhile observing the reduction of ΔE* for the MO_x covered PU fibers proving the screening effect of the designed systems.

Table 6
Parameters obtained from equation 24.

Sample	k_1	k_2	n
PU	0.22 ± 0.01^a	–	-0.12 ± 0.02^c
PU@Cu	0.95 ± 0.03^b	0.82 ± 0.03^a	0.83 ± 0.04^a
PU@Zn	0.95 ± 0.05^b	0.59 ± 0.08^b	0.37 ± 0.02^b
PU@Cu/Zn	1.06 ± 0.05^c	0.96 ± 0.08^a	0.89 ± 0.05^a

For each fiber membrane, different superscript letters in the same column indicate that the mean values are significantly different ($p \leq 0.05$).

3.3. Antibacterial activity

The antibacterial activity of the films PU@Cu, PU@Zn and PU@Cu/Zn was tested at 16, 20 and 24 h against both Gram-positive *Staphylococcus aureus* and Gram-negative *Escherichia coli* (Fig. 11).

The growth was evaluated by measuring the optical density (600 nm) and referred to that of the control sample (PU), the same material, but without metals. As reported in Fig. 11, films containing Cu or Zn exhibited significant antimicrobial activity versus *E. coli*, with PU@Cu slightly more effective. The antimicrobial effect reached its maximum value at 24 h, 98 and 92 % growth inhibition for PU@Cu and PU@Zn, respectively, but most of the toxic action occurred in the first 16 h, 88 and 83 % inhibition. The co-presence of both metals (PU@Cu/Zn) was not able to induce significant effects. The antimicrobial activity (A) estimated as the difference between growth values (logarithm to base 10) of control films and those containing the metals, at 24 h was of 1.1 for PU@Zn and 1.8 for PU@Cu [68]. Significant activity against *S. aureus* was also found, albeit with some differences. All three different metal-containing samples exhibited antimicrobial activity and the inhibitory effect on growth was very similar to each other; however, this was lower than that found for *E. coli*, ranging from 50 % and 62 % at 16 h and 86 % to 88 % at 24 h. The value of A reached a maximum of 1.0 (at 24 h) for all three different samples.

4. Conclusions

In this paper the design and fabrication of electrospun complex materials for a potential application in protective clothing was presented. The fiber membrane were prepared by using polyurethane which was modified with copper and zinc oxide as efficient UV screening materials. SEM micrographs, X-ray analysis and EDX proved the deposition of metal oxides onto PU electrospun fibers. The improvement of thermal stability has been proved by carrying out TGA and flame contact tests. To further demonstrate the potentialities of the designed materials in protective clothing field, barrier properties to water vapor and retention tests of different common liquids have been carried out demonstrating a reduction of permeability to water vapor which can be suitable for outdoor applications. Moreover, the fiber membranes seem to well stand against the permeation to acidic, basic and sweat simulant solutions. Transmittance spectra proved the decrease in transmission (about 99.8 %) along the whole wavelength range while the estimation of FTIR spectra as well as the calculation of carbonyl index gave a clear indication of UV stabilization against degradation induced by UV-rays. The cytotoxic effect against $Gram^+$ and $Gram^-$ bacteria was evaluated by choosing two bacterial strains, demonstrating an antimicrobial activity for Cu and Zn oxides covered TPU membranes while a slightly reduced activity was found for the Cu/Zn based PU fibers. The reported results allow for stating that the designed materials show great potential as high-performance materials for the fabrication of high-performance solutions for protective clothing.

Data Availability Statement: The raw/processed data required to reproduce these findings cannot be shared at this time as the data also forms part of an ongoing study.

CRediT authorship contribution statement

Gianluca Viscusi: Conceptualization, Formal analysis, Investigation, Data curation, Writing – review & editing. **Elena Lamberti:** Formal analysis, Investigation, Writing – review & editing. **Francesca D'Amico:** Data curation, Writing – review & editing. **Loredana Tammaro:** Formal analysis, Investigation, Writing – review & editing. **Giovanni Vigliotta:** Formal analysis, Investigation, Data curation, Writing – review &

Table 7
Chromaticity data of PU fiber membrane at 0 and 45 days.

Irradiation time (days)	0				45			
	L*	a*	b*	ΔE*	L*	a*	b*	ΔE*
PU	85.05	−0.61	10.87	0	88.87	−0.81	3.52	8.28 ± 0.29^{a}
PU@Cu	87.88	−5.19	5.91	0	89.64	−5.65	3.98	2.65 ± 0.06^{c}
PU@Zn	82.98	1.27	12.69	0	86.29	1.13	10.85	3.79 ± 0.16^{b}
PU@Cu/Zn	86.19	−27.81	−6.55	0	87.91	−29.65	−7.18	2.59 ± 0.01^{c}

For each fiber membrane, different superscript letters in the same column indicate that the mean values are significantly different ($p \leq 0.05$).

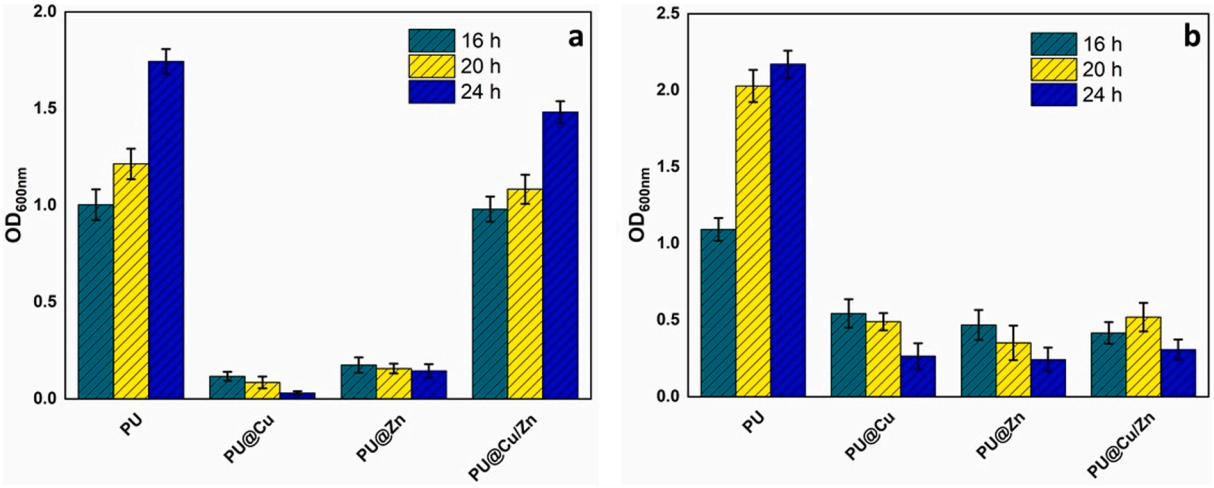

Fig. 11. Antimicrobial activity versus a) *E. coli* and b) *S. aureus*.

editing. **Giuliana Gorrasi:** Conceptualization, Funding acquisition.

Declaration of Competing Interest

The authors declare that they have no known competing financial interests or personal relationships that could have appeared to influence the work reported in this paper.

Data availability

No data was used for the research described in the article.

Project Prin 2017 "MultIFunctional poLymer cOmposites based on groWn matERials (MIFLOWER)" (grant number: 2017B7MMJ5_001) from the Italian Ministry of University and Research.

References

[1] A. El.shafei, A. Abou-Okeil, ZnO/carboxymethyl chitosan bionano-composite to impart antibacterial and UV protection for cotton fabric, Carbohydr. Polym. 83 (2011) 920–925. https://doi.org/10.1016/J.CARBPOL.2010.08.083.
[2] P.G. Parejo, M. Zayat, D. Levy, Highly efficient UV-absorbing thin-film coatings for protection of organic materials against photodegradation, J. Mater. Chem. 16 (2006) 2165–2169, https://doi.org/10.1039/B601577H.
[3] L. Xu, X. Zhang, Y. Shen, Y. Ding, L. Wang, Y. Sheng, Durable Superhydrophobic Cotton Textiles with Ultraviolet-blocking Property and Photocatalysis Based on Flower-Like Copper Sulfide (2018), https://doi.org/10.1021/acs.iecr.8b00254.
[4] H. Zhao, Q. Sun, J. Zhou, X. Deng, J. Cui, Switchable Cavitation: Switchable Cavitation in Silicone Coatings for Energy-Saving Cooling and Heating (Adv. Mater. 29/2020), Adv. Mater. 32 (2020) 2070215. https://doi.org/10.1002/ADMA.202070215.
[5] A.K. Sarkar, Textiles for UV protection, Text. Prot. (2005) 355–377, https://doi.org/10.1533/9781845690977.2.355.
[6] S. Lee, Developing UV-protective textiles based on electrospun zinc oxide nanocomposite fibers, Fibers Polym. 2009 103. 10 (2009) 295–301. https://doi.org/10.1007/S12221-009-0295-2.
[7] M. Sasani Ghamsari 1 Sanaz Alamdari, W. Han, H.-H. Park, Impact of nanostructured thin ZnO film in ultraviolet protection, Int. J. Nanomedicine. (2017) 12–207. https://doi.org/10.2147/IJN.S118637.
[8] R. Kaur, N.S. Thakur, S. Chandna, J. Bhaumik, Development of agri-biomass based lignin derived zinc oxide nanocomposites as promising UV protectant-cum-antimicrobial agents, J. Mater. Chem. B. 8 (2020) 260–269, https://doi.org/10.1039/C9TB01569H.
[9] O.S. Kushwaha, C.V. Avadhani, R.P. Singh, Preparation and characterization of self-photostabilizing UV-durable bionanocomposite membranes for outdoor applications, Carbohydr. Polym. 123 (2015) 164–173, https://doi.org/10.1016/J.CARBPOL.2014.12.062.
[10] H. Cui, M. Zayat, P.G. Parejo, D. Levy, Highly Efficient Inorganic Transparent UV-Protective Thin-Film Coating by Low Temperature Sol-Gel Procedure for Application on Heat-Sensitive Substrates, Adv. Mater. 20 (2008) 65–68, https://doi.org/10.1002/ADMA.200701960.
[11] D. Valerini, L. Tammaro, R. Vitali, G. Guillot, A. Rinaldi, Sputter-Deposited Ag Nanoparticles on Electrospun PCL Scaffolds: Morphology, Wettability and Antibacterial Activity, Coatings 2021, Vol. 11, Page 345. 11 (2021) 345. https://doi.org/10.3390/COATINGS11030345.
[12] S. Agarwal, J.H. Wendorff, A. Greiner, Use of electrospinning technique for biomedical applications, Polymer (Guildf). 49 (2008) 5603–5621, https://doi.org/10.1016/j.polymer.2008.09.014.
[13] T.J. Sill, H.A. von Recum, Electrospinning: Applications in drug delivery and tissue engineering, Biomaterials. 29 (2008) 1989–2006, https://doi.org/10.1016/j.biomaterials.2008.01.011.
[14] G. Gorrasi, R. Longo, G. Viscusi, Fabrication and characterization of electrospun membranes based on "poly(ε-caprolactone)", "poly(3-hydroxybutyrate)" and their blend for tunable drug delivery of curcumin, Polymers (Basel). 12 (2020) 1–16, https://doi.org/10.3390/polym12102239.
[15] A.P. Kishan, E.M. Cosgriff-Hernandez, Recent advancements in electrospinning design for tissue engineering applications: A review, J. Biomed. Mater. Res. - Part A. 105 (2017) 2892–2905, https://doi.org/10.1002/jbm.a.36124.
[16] C. Liu, P.C. Hsu, H.W. Lee, M. Ye, G. Zheng, N. Liu, W. Li, Y. Cui, Transparent air filter for high-efficiency PM2.5 capture, Nat. Commun. 2015 61. 6 (2015) 1–9. https://doi.org/10.1038/ncomms7205.
[17] N. Charernsriwilaiwat, P. Opanasopit, T. Rojanarata, T. Ngawhirunpat, P. Supaphol, Preparation and characterization of chitosan-hydroxybenzotriazole/polyvinyl alcohol blend nanofibers by the electrospinning technique, Carbohydr. Polym. 81 (2010) 675–680, https://doi.org/10.1016/j.carbpol.2010.03.031.
[18] P. Chegoonian, M. Feiz, S.A.H. Ravandi, S. Mallakpour, Preparation of sulfonated poly(ethylene terephthalate) submicron fibrous membranes for removal of basic dyes, J. Appl. Polym. Sci. 124 (2012), https://doi.org/10.1002/app.35167.
[19] C. Ribeiro, V. Sencadas, J.L.G. Ribelles, S. Lanceros-Méndez, Influence of processing conditions on polymorphism and nanofiber morphology of electroactive poly(vinylidene fluoride) electrospun membranes, Soft Mater. 8 (2010) 274–287, https://doi.org/10.1080/1539445X.2010.495630.
[20] J. Passaro, C. Imparato, D. Parida, A. Bifulco, F. Branda, A. Aronne, Electrospinning of PVP-based ternary composites containing SiO2 nanoparticles and hybrid TiO2 microparticles with adsorbed superoxide radicals, Compos. Part B Eng. 238 (2022), 109874, https://doi.org/10.1016/J.COMPOSITESB.2022.109874.

[21] G. Viscusi, E. Lamberti, V. Vittoria, G. Gorrasi, Coaxial electrospun membranes of poly(ε-caprolactone)/poly(lactic acid) with reverse core-shell structures loaded with curcumin as tunable drug delivery systems, Polym. Adv. Technol. (2021), https://doi.org/10.1002/PAT.5404.

[22] A. Di Salle, G. Viscusi, F. Di Cristo, A. Valentino, G. Gorrasi, E. Lamberti, V. Vittoria, A. Calarco, G. Peluso, Antimicrobial and Antibiofilm Activity of Curcumin-Loaded Electrospun Nanofibers for the Prevention of the Biofilm-Associated Infections, Molecules. 26 (2021), https://doi.org/10.3390/MOLECULES26164866.

[23] S. Zhang, H. Liu, J. Yu, B. Li, B. Ding, Multi-functional flexible 2D carbon nanostructured networks, Nat. Commun. 2020 111. 11 (2020) 1–8. https://doi.org/10.1038/s41467-020-18977-6.

[24] S. Zhang, H. Liu, N. Tang, N. Ali, J. Yu, B. Ding, Highly Efficient, Transparent, and Multifunctional Air Filters Using Self-Assembled 2D Nanoarchitectured Fibrous Networks, ACS Nano. (2019), https://doi.org/10.1021/ACSNANO.9B07293/SUPPL_FILE/NN9B07293_SI_002.MP4.

[25] Y. Zhang, Y. Zhang, Y. Liu, X. Wang, B. Yang, A novel surface modification of carbon fiber for high-performance thermoplastic polyurethane composites, Appl. Surf. Sci. 382 (2016) 144–154, https://doi.org/10.1016/J.APSUSC.2016.04.118.

[26] G. Viscusi, F. D'Amico, G. Gorrasi, In situ one-step fabrication of layered double hydroxide deposited on cellulose: Effect of modified cellulose on physical properties of polyurethane composites, Polym. Adv. Technol. 33 (2022) 2300–2312, https://doi.org/10.1002/PAT.5684.

[27] J. Gao, L. Wang, Z. Guo, B. Li, H. Wang, J. Luo, X. Huang, H. Xue, Flexible, superhydrophobic, and electrically conductive polymer nanofiber composite for multifunctional sensing applications, Chem. Eng. J. 381 (2020), 122778, https://doi.org/10.1016/J.CEJ.2019.122778.

[28] M. Kotal, S.K. Srivastava, S.K. Manu, Layered double hydroxide as nanofiller in the development of polyurethane nanocomposites, J. Nanosci. Nanotechnol. 10 (2010) 5730–5740, https://doi.org/10.1166/JNN.2010.2455.

[29] S. Zhang, F. Chu, Z. Xu, Y. Zhou, Y. Qiu, L. Qian, Y. Hu, B. Wang, W. Hu, The improvement of fire safety performance of flexible polyurethane foam by Highly-efficient P-N-S elemental hybrid synergistic flame retardant, J. Colloid Interface Sci. 606 (2022) 768–783, https://doi.org/10.1016/J.JCIS.2021.08.069.

[30] Z. Ma, Q. Li, J. Wei, C. Liang, T. Yang, G. Wang, C. Xia, Effects of Al-based alloy powders on the mechanical behavior, corrosion resistance and infrared emissivity of polyurethane composite coatings, Colloids Surfaces A Physicochem. Eng. Asp. 624 (2021), 126782, https://doi.org/10.1016/J.COLSURFA.2021.126782.

[31] M. Dai, J. Wang, Y. Zhang, Improving water resistance of waterborne polyurethane coating with high transparency and good mechanical properties, Colloids Surfaces A Physicochem. Eng. Asp. 601 (2020), 124994, https://doi.org/10.1016/J.COLSURFA.2020.124994.

[32] S.M. Sapuan, F.L. Pua, Y.A. El-Shekeil, F.M. AL-Oqla, Mechanical properties of soil buried kenaf fibre reinforced thermoplastic polyurethane composites, Mater. Des. 50 (2013) 467–470. https://doi.org/10.1016/J.MATDES.2013.03.013.

[33] F.J. Davis, G.R. Mitchell, Polyurethane Based Materials with Applications in Medical Devices, Bio-Materials Prototyp, Appl. Med. (2008) 27–48, https://doi.org/10.1007/978-0-387-47683-4_3.

[34] H. Tian, Y. Yao, S. Zhang, Y. Wang, A. Xiang, Enhanced thermal stability and flame resistance of rigid polyurethane-imide foams by varying copolymer composition, Polym. Test. 67 (2018) 68–74, https://doi.org/10.1016/J.POLYMERTESTING.2018.02.020.

[35] X.F. Yang, J. Li, S.G. Croll, D.E. Tallman, G.P. Bierwagen, Degradation of low gloss polyurethane aircraft coatings under UV and prohesion alternating exposures, Polym. Degrad. Stab. 80 (2003) 51–58, https://doi.org/10.1016/S0141-3910(02)00382-8.

[36] D. Rosu, L. Rosu, C.N. Cascaval, IR-change and yellowing of polyurethane as a result of UV irradiation, Polym. Degrad. Stab. 94 (2009) 591–596, https://doi.org/10.1016/J.POLYMDEGRADSTAB.2009.01.013.

[37] S. Sundarrajan, S. Ramakrishna, The use of nanomaterials in smart protective clothing, Smart Text, Prot. (2013) 127–147, https://doi.org/10.1533/9780857097620.1.127.

[38] S. Karagoz, N. Burak Kiremitler, G. Sarp, S. Pekdemir, S. Salem, A.G. Goksu, M. Serdar Onses, I. Sozdutmaz, E. Sahmetlioglu, E.S. Ozkara, A. Ceylan, E. Yilmaz, Antibacterial, antiviral, and self-cleaning mats with sensing capabilities based on electrospun nanofibers decorated with ZnO nanorods and Ag nanoparticles for protective clothing applications, ACS Appl. Mater. Interfaces. 13 (2021) 5678–5690, https://doi.org/10.1021/ACSAMI.0C15606/ASSET/IMAGES/LARGE/AM0C15606_0009.JPEG.

[39] S. Lee, Developing UV-protective textiles based on electrospun zinc oxide nanocomposite fibers, Fibers Polym. 10 (2009) 295–301, https://doi.org/10.1007/S12221-009-0295-2.

[40] N. Karim, S. Afroj, K. Lloyd, L.C. Oaten, D.V. Andreeva, C. Carr, A.D. Farmery, I.-D. Kim, K.S. Novoselov, Sustainable Personal Protective Clothing for Healthcare Applications: A Review, ACS Nano. 14 (2020), https://doi.org/10.1021/acsnano.0c05537.

[41] F.D.S. Larotonda, K.N. Matsui, P.J.A. Sobral, J.B. Laurindo, Hygroscopicity and water vapor permeability of Kraft paper impregnated with starch acetate, J. Food Eng. 71 (2005) 394–402, https://doi.org/10.1016/j.jfoodeng.2004.11.002.

[42] B. Saberi, Q. Vuong, S. Chockchaisawasdee, J. Golding, C. Scarlett, C. Stathopoulos, Water Sorption Isotherm of Pea Starch Edible Films and Prediction Models, Foods. 5 (2015) 1, https://doi.org/10.3390/foods5010001.

[43] J. Chirife, R. Boquet, C.F. Fontàn, H.A. Iglesias, A New Model for Describing the Water Sorption Isotherm of Foods, J. Food Sci. 48 (1983) 1382–1383, https://doi.org/10.1111/j.1365-2621.1983.tb09245.x.

[44] G. Viscusi, R. Adami, G. Gorrasi, Fabrication of rice flour films reinforced with hemp hurd and loaded with grapefruit seed oil: A simple way to valorize agro-waste resources toward low cost materials with added value, Ind. Crops Prod. 170 (2021), 113785, https://doi.org/10.1016/J.INDCROP.2021.113785.

[45] G. Viscusi, R. Pantani, G. Gorrasi, Transport properties of water vapor through hemp fibers modified with a sustainable process: Effect of surface morphology on the thermodynamic and kinetic phenomena, Appl. Surf. Sci. 541 (2021), 148433, https://doi.org/10.1016/j.apsusc.2020.148433.

[46] G.K. Van Der Wel, O.C.G. Adan, Moisture in organic coatings - a review, Prog. Org. Coatings. 37 (1999) 1–14, https://doi.org/10.1016/S0300-9440(99)00058-2.

[47] J.L. Lundberg, MOLECULAR CLUSTERING AND SEGREGATION IN SORPTION SYSTEMS, 1972.

[48] A. Kriaa, N. Hamdi, E. Srasra, Determination Of Point Of Zero Charge Of Tunisian Kaolinites By Potentiometric And Mass Titration Methods, accessed August 17, 2021, Anal. Chem. An Indian J. 2 (2008), https://www.tsijournals.com/abstract/determination-of-point-of-zero-charge-of-tunisian-kaolinites-by-potentiometric-and-mass-titration-methods-19.html.

[49] M.P. Elizalde-González, L.E. García-Díaz, Application of a Taguchi L16 orthogonal array for optimizing the removal of Acid Orange 8 using carbon with a low specific surface area, Chem. Eng. J. 163 (2010) 55–61, https://doi.org/10.1016/J.CEJ.2010.07.040.

[50] R. Shanti, A.N. Hadi, Y.S. Salim, S.Y. Chee, S. Ramesh, K. Ramesh, Degradation of ultra-high molecular weight poly(methyl methacrylate- co -butyl acrylate- co -acrylic acid) under ultra violet irradiation, RSC Adv. 7 (2016) 112–120, https://doi.org/10.1039/C6RA25313J.

[51] A. Verdino, G. Vigliotta, D. Giordano, I. Caputo, A. Soriente, M. De Rosa, A. Marabotti, Synthesis and biological evaluation of the progenitor of a new class of cephalosporin analogues, with a particular focus on structure-based computational analysis, PLoS One. 12 (2017) e0181563.

[52] B. Wang, J. Li, G. Wang, W. Liang, Y. Zhang, L. Shi, Z. Guo, W. Liu, Methodology for Robust Superhydrophobic Fabrics and Sponges from In Situ Growth of Transition Metal/Metal Oxide Nanocrystals with Thiol Modification and Their Applications in Oil/Water Separation (2013), https://doi.org/10.1021/am303176a.

[53] R. Venkatakrishnan, T. Senthilvelan, T. Vijayakumar, Characterization of Polyurethane Coated Aerospace Aluminium Alloy (7075) By DSC, XRD and Adhesion Test, J Appl Mech Eng. 6 (2017) 6, https://doi.org/10.4172/2168-9873.1000296.

[54] S. Talam, S.R. Karumuri, N. Gunnam, Synthesis Characterization, and Spectroscopic Properties of ZnO Nanoparticles, ISRN Nanotechnol. 2012 (2012) 1–6, https://doi.org/10.5402/2012/372505.

[55] P.K. Raul, S. Senapati, A.K. Sahoo, I.M. Umlong, R.R. Devi, A.J. Thakur, V. Veer, CuO nanorods: A potential and efficient adsorbent in water purification, RSC Adv. 4 (2014) 40580–40587, https://doi.org/10.1039/C4RA04619F.

[56] C. Miranda, J. Castaño, E. Valdebenito-Rolack, F. Sanhueza, R. Toro, H. Bello-Toledo, P. Uarac, L. Saez, Copper-Polyurethane Composite Materials: Particle Size Effect on the Physical-Chemical and Antibacterial Properties, Polymers (Basel). 12 (2020), https://doi.org/10.3390/POLYM12091934.

[57] Y. Fang, J. Li, X. Du, Z. Du, X. Cheng, H. Wang, Thermal- and mechanical-responsive polyurethane elastomers with self-healing, mechanical-reinforced, and thermal-stable capabilities, Polymer (Guildf). 158 (2018) 166–175, https://doi.org/10.1016/J.POLYMER.2018.10.056.

[58] D. Tabuani, F. Bellucci, A. Terenzi, G. Camino, Flame retarded Thermoplastic Polyurethane (TPU) for cable jacketing application, Polym. Degrad. Stab. 97 (2012) 2594–2601, https://doi.org/10.1016/J.POLYMDEGRADSTAB.2012.07.011.

[59] M. Villani, R. Consonni, M. Canetti, F. Bertoglio, S. Iervese, G. Bruni, L. Visai, S. Iannace, F. Bertini, Polyurethane-Based Composites: Effects of Antibacterial Fillers on the Physical-Mechanical Behavior of Thermoplastic Polyurethanes, Polym. 2020, Vol. 12, Page 362. 12 (2020) 362. https://doi.org/10.3390/POLYM12020362.

[60] Y. Peng, W. Wang, J. Cao, X. Guo, Effects of a layered double hydroxide (LDH) on the photostability of wood flour/polypropylene composites during UV weathering, RSC Adv. 5 (2015) 41230–41237, https://doi.org/10.1039/C5RA04999G.

[61] S. Brunauer, L.S. Deming, W.E. Deming, E. Teller, On a Theory of the van der Waals Adsorption of Gases, J. Am. Chem. Soc. 62 (1940) 1723–1732, https://doi.org/10.1021/ja01864a025.

[62] G. Gorrasi, L. Tammaro, M. Tortora, V. Vittoria, D. Kaempfer, P. Reichert, R. Mülhaupt, Transport properties of organic vapors in nanocomposites of isotactic polypropylene, J. Polym. Sci. Part B Polym. Phys. 41 (2003) 1798–1805, https://doi.org/10.1002/POLB.10541.

[63] J. Xu, T. Hao, C. Liu, J. Bi, J. Sun, Z. Wen, Z. Hou, J. Wei, pH-Responsive and degradable polyurethane film with good tensile properties for drug delivery in vitro, Mater. Today Commun. 29 (2021), 102969, https://doi.org/10.1016/J.MTCOMM.2021.102969.

[64] F. Xie, T. Zhang, P. Bryant, V. Kurusingal, J.M. Colwell, B. Laycock, Degradation and stabilization of polyurethane elastomers, Prog. Polym. Sci. 90 (2019) 211–268, https://doi.org/10.1016/J.PROGPOLYMSCI.2018.12.003.

[65] J.F. Rabek, Photodegradation and photo-oxidative degradation of heterochain polymers, 1st ed., Springer, Dordrecht, 1995. https://doi.org/10.1007/978-94-011-1274-1_4.

[66] M.F. Sonnenschein, Polyurethane Building Blocks, Polyurethanes. (2014) 10–104. https://doi.org/10.1002/9781118901274.CH2.
[67] C. Wilhelm, A. Rivaton, J.L. Gardette, Infrared analysis of the photochemical behaviour of segmented polyurethanes: 3. Aromatic diisocyanate based polymers, Polymer (Guildf). 39 (1998) 1223–1232, https://doi.org/10.1016/S0032-3861(97)00353-4.
[68] D. Valerini, L. Tammaro, F. Villani, A. Rizzo, I. Caputo, G. Paolella, G. Vigliotta, Antibacterial Al-doped ZnO coatings on PLA films, J. Mater. Sci. 2020 5511. 55 (2020) 4830–4847. https://doi.org/10.1007/S10853-019-04311-Z.